

A Meshless Local Petrov-Galerkin (MLPG) Formulation for Static and Free Vibration Analyses of Thin Plates

Y. T. Gu and G. R. Liu¹

Abstract: A meshless method for the analysis of Kirchhoff plates based on the Meshless Local Petrov-Galerkin (MLPG) concept is presented. A MLPG formulation is developed for static and free vibration analyses of thin plates. Local weak form is derived using the weighted residual method in local supported domains from the 4th order partial differential equation of Kirchhoff plates. The integration of the local weak form is performed in a regular-shaped local domain. The Moving Least Squares (MLS) approximation is used to construct shape functions. The satisfaction of the high continuity requirements is easily met by MLS interpolant, which is based on a weight function with high continuity and a quadratic polynomial basis. The validity and efficiency of the present MLPG method are demonstrated through a number of examples of thin plates under various loads and boundary conditions. Some important parameters on the performance of the present method are investigated thoroughly in this paper. The present method is also compared with EFG method and Finite Element Method in terms of robustness and performance.

keyword: Meshless Method; Meshless Local Petrov-Galerkin (MLPG) method; Kirchhoff plates; Free Vibration; Numerical Analysis

1 Introduction

With the wide use of plate structures, analyses of plates become very important. Exact analyses of plates are usually very limited. Therefore, numerical techniques with different discretization schemes, such as Finite Element Method (FEM), are widely used in these analyses. How-

ever, in FEM, a mesh must be required to establish element connectivity to form element equations.

Meshless method has attracted more and more attention from researchers in recent years, and it is regarded as a potential numerical method in computational mechanics, as it does not require a mesh to discretize the problem domain, and the approximate solution is constructed entirely based on a set of scattered nodes. Several meshless methods, such as Diffuse Element Method (DEM) [Nayroles et al. (1992)], Element Free Galerkin (EFG) method [Belytschko et al. (1994)], Finite Node (FN) method [Oñate et al. (1996); Wordelman et al. (2000)], Reproducing Kernel Particle Method (RKPM) [Liu et al. (1995)], Point Interpolation Method (PIM) [Liu and Gu (2001a)], Point Assembly Method (PAM) [Liu (1999)], Boundary Node Method (BNM) [Mukherjee and Mukherjee (1997)] have been proposed and achieved remarkable progress in solving a wide range of static and dynamic problems for solids and structures. Techniques of coupling meshless methods with other established numerical methods have also been proposed, such as coupled EFG/FEM [Belytschko and Organ (1995)], EFG/Boundary Element Method (BEM) [Liu and Gu (2000a); Gu and Liu (2001a)].

The above-mentioned meshless methods are all based on global weak forms or Boundary Integral Equation (BIE). In particular, these meshless methods are “meshless” only in terms of the interpolation of the field or boundary variables, as compared to the usual FEM or Boundary Element Method (BEM). These meshless methods have to use background cells to integrate a weak form over the global problem domain and boundary.

Some research work have been done for alleviating the global integration background cells. Truly meshless methods, called the Meshless Local Petrov-Galerkin (MLPG) method [Atluri and Zhu (1998), (2000a,b); Atluri et al. (1999a,b); Kim and Atluri (2000)], the Local Boundary Integral Equation (LBIE) method [Zhu et

¹ Correspondence to: Gui-Rong LIU

E-mail: mpeliugr@nus.edu.sg, engp8973@nus.edu.sg

Centre for Advanced Computations in Engineering Science

c/o: Dept. of Mechanical Engineering, National University of Singapore

10 Kent Ridge Crescent, Singapore 119260

<http://www.nus.edu.sg/ACES>

al. (1998)], and the Local Point Interpolation Method (LPIM) [Liu and Gu (2001b)] have been developed. These meshless methods don't need any "element" or "mesh" for both field interpolation and background integration. Therefore, they are so-called "truly" meshless methods.

The MLPG concept is proposed by Atluri and his colleagues. In the MLPG, a local weak form is proposed by locally using weighted residual method. The integration for the local weak form is only based on a regular-shaped local domain (such as spheres, rectangular, and ellipsoids). Therefore, the global integration background cells are not needed. The Moving Least Squares (MLS) approximation is used to construct shape functions. The detailed assessment of MLPG method is presented in a paper by Atluri et al. [Atluri et al. (1999b)]. The MLPG method has been successfully used for one-dimensional 4th order thin beam static analysis [Atluri et al. (1999a)], two-dimensional elasto-static analysis [Atluri and Zhu (2000b); Chang and Batra (2001)] and dynamic analysis [Gu and Liu (2001b)], fluid mechanics and potential problems [Lin and Atluri (2000); Lin and Atluri (2001)]. In addition, the MLPG method has been combined with finite element method or boundary element method [Liu and Gu (2000b)].

The goal of the present paper is to develop the MLPG formulation for static and free vibration analyses of thin plates. Studies have been reported on solving the plate problem by the EFG method [Krysl and Belytschko (1995); Liu and Chen (2001)]. In the Kirchhoff plate theory, which leads a 4th order partial differential equation, the high continuity in trial functions is required. Atluri et al. (1999a) proposed a generalized moving least squares (GMLS) formulation to incorporate the information concerning the derivative of the field variable into the interpolation scheme. The GMLS has been used in analyses of 1-D thin beams, and it also can be extended to the analysis of thin plates. However, the requirement of high continuity can be easily satisfied by the traditional MLS interpolation, in which no derivative term of the field variable is included. The continuity of the shape functions is primarily governed by the continuity of the weight function. Therefore, as it is not difficult to construct sufficiently smooth weight functions, the high continuity requirements can be easily satisfied by the traditional MLS interpolation. The numerical approach can be greatly simplified by use of the traditional MLS ap-

proximation.

In this paper, a MLPG formulation is proposed for static and free vibration analyses of thin plates. The local weak form is developed using weighted residual method locally from the 4th order partial differential equation of Kirchhoff plates. The Moving Least Squares approximation is used to construct shape functions with the high continuity. Several examples of static and free vibration analyses of thin plates under various loads and boundary conditions are presented to demonstrate the convergence, validity and efficiency of the present method. Some important parameters on the performance of the present method are investigated thoroughly in this paper. The present method is also compared with EFG method and FEM in terms of robustness and performance.

2 Governing equations

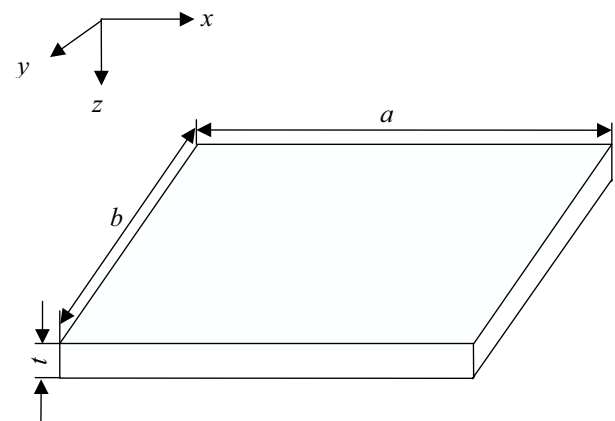


Figure 1 : Thin plate and its coordinate system

Consider a Kirchhoff plate shown in Fig. 1. A Cartesian coordinate system is used. The classical theory of thin plates is based on the displacement field

$$\begin{aligned} u_x(x, y, z) &= u - z \frac{\partial w}{\partial x} & u_y(x, y, z) &= u - z \frac{\partial w}{\partial y}, \\ u_z(x, y, z) &= w(x, y) \end{aligned} \quad (1)$$

where (u_x, u_y, u_z) denote the displacements of the point (x, y, z) along the x, y and z directions, and (u, v, w) represent displacements of a point on the midplane $(x, y, 0)$. The slope, θ , is also the function of w , $\theta_i = \frac{\partial w}{\partial x_i}$. Therefore, w can be taken as only an independent variable. The

partial differential equation [Reddy (1993)] governing w for static and free vibration analyses of thin plates is

$$\begin{aligned} & \frac{\partial^2}{\partial x^2} (D_{11} \frac{\partial^2 w}{\partial x^2} + D_{12} \frac{\partial^2 w}{\partial y^2}) + \frac{\partial^2}{\partial y^2} (D_{12} \frac{\partial^2 w}{\partial x^2} + D_{22} \frac{\partial^2 w}{\partial y^2}) \\ & + 2 \frac{\partial^2}{\partial x \partial y} (2D_{66} \frac{\partial^2 w}{\partial x \partial y}) - f(x, y) + I_0 \frac{\partial^2 w}{\partial t^2} \\ & - I_2 \frac{\partial^2}{\partial t^2} (\frac{\partial w}{\partial x} + \frac{\partial w}{\partial y}) = 0 \quad \text{in } \Omega \end{aligned} \quad (2)$$

where D_{ij} are the plate rigidities

$$D_{11}=D_{22}=\frac{Et^3}{12(1-\nu^2)}, \quad D_{12}=\nu D_{11}, \quad D_{66}=\frac{Gt^3}{12}, \quad (3a)$$

for isotropic material and I_0 and I_2 are the mass moments of inertia:

$$I_0 = \int_{-h/2}^{h/2} \rho dz = \rho h, \quad I_2 = \int_{-h/2}^{h/2} \rho z^2 dz = \rho h^3 / 12 \quad (3b)$$

The boundary conditions are give at global boundary, Γ as

essential boundary conditions:

$$w = \bar{w}, \text{ on } \Gamma_w; \theta_n = \frac{\partial w}{\partial n} = \bar{\theta}, \text{ on } \Gamma_\theta \quad (4)$$

natural boundary conditions: $M_n = \bar{M}$, on Γ_m ; $V_n = \bar{V}$, on Γ_V

where M and V denote the moment and the equivalent shear force. Γ_w , Γ_θ , Γ_M and Γ_V denote the boundaries where deflection, slope, moment, and shear force are specified, respectively. n is the unit outward normal to domain Ω .

3 Moving Least Squares

In this paper, the moving least squares approximation is employed [Lancaster and Salkauskas (1981)]. Consider a thin plate domain Ω The MLS interpolant $w^h(x)$ is defined in the domain Ω_y

$$w^h(\mathbf{x}) = \sum_{j=1}^m p_j(\mathbf{x}) a_j(\mathbf{x}) = \mathbf{p}^T(\mathbf{x}) \mathbf{a}(\mathbf{x}) \quad (5)$$

where $\mathbf{p}(\mathbf{x})$ called basis functions is considered in the space coordinates $\mathbf{x}^T=[x, y]$. m is the number of basis functions. The quadratic polynomial basis functions in two-dimension is given by

$$\mathbf{p}^T(\mathbf{x}) = [1, x, y, x^2, xy, y^2] \quad m = 6 \quad (6)$$

The coefficient $a_j(x)$ in equation (5) is also functions of \mathbf{x} . $\mathbf{a}(\mathbf{x})$ is obtained at any point \mathbf{x} by minimizing a weighted discrete L_2 norm of:

$$J = \sum_{i=1}^n v(\mathbf{x} - \mathbf{x}_i) [\mathbf{p}^T(\mathbf{x}_i) \mathbf{a}(\mathbf{x}) - w_i]^2 \quad (7)$$

where n is the number of points in the neighborhood of \mathbf{x} for which the weight function $v(\mathbf{x} - \mathbf{x}_i) \neq 0$, and w_i is the nodal value of w at $\mathbf{x}=\mathbf{x}_i$.

The stationarity of J with respect to $\mathbf{a}(\mathbf{x})$ leads to the following linear relation between $\mathbf{a}(\mathbf{x})$ and w_i :

$$\mathbf{A}(\mathbf{x}) \mathbf{a}(\mathbf{x}) = \mathbf{B}(\mathbf{x}) \mathbf{w} \quad (8)$$

Solving $\mathbf{a}(\mathbf{x})$ from equation (8) and substituting it into equation (5), we have

$$w^h(\mathbf{x}) = \sum_{i=1}^n \phi_i(\mathbf{x}) w_i \quad (9)$$

where the MLS shape function $\phi(\mathbf{x})$ is defined by

$$\phi_i(\mathbf{x}) = \sum_{j=1}^m p_j(\mathbf{x}) (\mathbf{A}^{-1}(\mathbf{x}) \mathbf{B}(\mathbf{x}))_{ji} \quad (10)$$

where $\mathbf{A}(\mathbf{x})$ and $\mathbf{B}(\mathbf{x})$ are the matrices defined by

$$\mathbf{A}(\mathbf{x}) = \sum_{i=1}^n v_i(\mathbf{x}) \mathbf{p}^T(\mathbf{x}_i) \mathbf{p}(\mathbf{x}_i), \quad v_i(x) = v(\mathbf{x} - \mathbf{x}_i) \quad (11)$$

$$\mathbf{B}(\mathbf{x}) = [v_1(\mathbf{x})\mathbf{p}(\mathbf{x}_1), v_2(\mathbf{x})\mathbf{p}(\mathbf{x}_2), \dots, v_n(\mathbf{x})\mathbf{p}(\mathbf{x}_n)] \quad (12) \quad (16)$$

It can be found from above discussion that the MLS approximation does not pass through the nodal parameter values. Therefore the MLS shape functions given in equation (10) do not, in general, satisfy the Kronecker delta condition.

For convenience to obtain the partial derivatives of shape functions, equation (10) is re-written as

$$\Phi(\mathbf{x}) = \gamma^T(\mathbf{x})\mathbf{B}(\mathbf{x}) \quad (13a)$$

$$\mathbf{A}\gamma = \mathbf{P} \quad (13b)$$

The partial derivatives of γ can be obtained as follows:

$$\mathbf{A}\gamma_{,i} = \mathbf{P}_{,i} - \mathbf{A}_{,i}\gamma \quad (14a)$$

$$\mathbf{A}\gamma_{,ij} = \mathbf{P}_{,ij} - (\mathbf{A}_{,i}\gamma_{,j} + \mathbf{A}_{,j}\gamma_{,i} + \mathbf{A}_{,ij}\gamma) \quad (14b)$$

$$\begin{aligned} \mathbf{A}\gamma_{,ijk} = & \mathbf{P}_{,ijk} - (\mathbf{A}_{,i}\gamma_{,jk} + \mathbf{A}_{,j}\gamma_{,ik} + \mathbf{A}_{,k}\gamma_{,ij} + \mathbf{A}_{,ij}\gamma_{,k} \\ & + \mathbf{A}_{,ik}\gamma_{,j} + \mathbf{A}_{,jk}\gamma_{,i} + \mathbf{A}_{,ijk}\gamma) \end{aligned} \quad (14c)$$

where i, j and k denote coordinate x and y . A comma designates a partial derivative with respect to the indicated spatial variable. The partial derivatives of shape function Φ can be obtained as follows:

$$\Phi_{,i} = \gamma_{,i}\mathbf{B} + \gamma\mathbf{B}_{,i} \quad (15a)$$

$$\Phi_{,ij} = \gamma_{,ij}\mathbf{B} + \gamma_{,i}\mathbf{B}_{,j} + \gamma_{,j}\mathbf{B}_{,i} + \gamma\mathbf{B}_{,ij} \quad (15b)$$

$$\begin{aligned} \Phi_{,ijk} = & \gamma_{,ijk}\mathbf{B} + \gamma_{,ij}\mathbf{B}_{,k} + \gamma_{,ik}\mathbf{B}_{,j} + \gamma_{,jk}\mathbf{B}_{,i} + \gamma_{,i}\mathbf{B}_{,jk} \\ & + \gamma_{,j}\mathbf{B}_{,ik} + \gamma_{,k}\mathbf{B}_{,ij} + \gamma\mathbf{B}_{,ijk} \end{aligned} \quad (15c)$$

From equation (10), it can be found that the continuity of the shape function Φ is governed by the continuity of the basis function p_j , and by the smoothness of the matrices \mathbf{A} and \mathbf{B} . The latter is governed by the smoothness of the weight function. Therefore, the choice of weight function plays an important role in the performance of the MLS approximation. In this paper, the following 4-orders spline function is used:

$$v_i(x) = \begin{cases} 1 - 6\left(\frac{d_i}{r_v}\right)^2 + 8\left(\frac{d_i}{r_v}\right)^3 - 3\left(\frac{d_i}{r_v}\right)^4 & 0 \leq d_i \leq r_v \\ 0 & d_i \geq r_v \end{cases}$$

Where $d_i = |\mathbf{x}_Q - \mathbf{x}_i|$ is the distance from node \mathbf{x}_i to the sampling point \mathbf{x}_Q , r_v is the size of the support for the weight function. The weight function possesses 4-order continuity in the support domain and the boundaries of support domain.

In MLS approximation, the number of nodes, n , chosen in the influence domain should ensure matrix \mathbf{A} in equation (10) invertible and the interpolation accurate. The reasonable n depends on the problem and the number of basis function, m . It is usually no theoretical best value of n . In general, the parameter can be determined by numerical examination.

4 Local weak form of MLPG

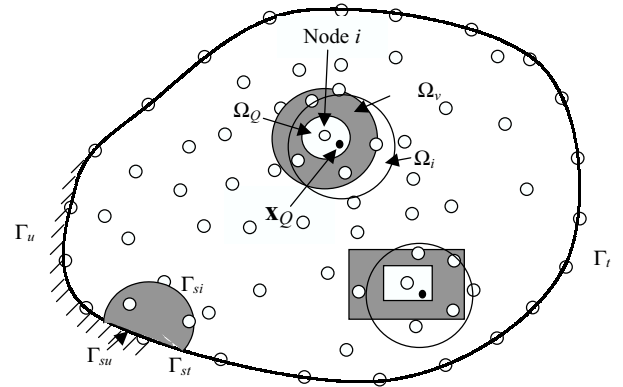


Figure 2 : The support domain Ω_v and integration domain Ω_0 for node i ; the interpolation domain Ω_i for Gauss integration point \mathbf{x}_Q

The penalty method is used to enforce the essential boundary condition. A local weak form of equation (2), over a local subdomain Ω_i bounded by Γ_s , can be obtained using the weighted residual method.

$$\begin{aligned} \int_{\Omega_s} \left\{ \frac{\partial^2}{\partial x^2} (D_{11} \frac{\partial^2 w}{\partial x^2} + D_{12} \frac{\partial^2 w}{\partial y^2}) + \frac{\partial^2}{\partial y^2} (D_{12} \frac{\partial^2 w}{\partial x^2} + D_{22} \frac{\partial^2 w}{\partial y^2}) \right. \\ \left. + 2 \frac{\partial^2}{\partial x \partial y} (2D_{66} \frac{\partial^2 w}{\partial x \partial y}) - f(x, y) + I_0 \frac{\partial^2 w}{\partial t^2} - I_2 \frac{\partial^2}{\partial t^2} \left(\frac{\partial w}{\partial x} + \frac{\partial w}{\partial y} \right) \right\} d\Omega \\ \left\{ - \int_{\Gamma_{sw}} \alpha v (w - \bar{w}) d\Gamma - \int_{\Gamma_{s\theta}} \beta \frac{\partial v}{\partial n} (\theta_n - \bar{\theta}) d\Gamma = 0 \right. \end{aligned} \quad (17)$$

where v is the weight function. α and β are the penalty constant for deflection and slope, respectively. The values of α and β can be taken as the range of the young's modulus.

Equation (17) can be integrated by parts to become

$$\begin{aligned} & \int_{\Omega_s} \left\{ \frac{\partial^2 v}{\partial x^2} (D_{11} \frac{\partial^2 w}{\partial x^2} + D_{12} \frac{\partial^2 w}{\partial y^2}) + \frac{\partial^2 v}{\partial y^2} (D_{12} \frac{\partial^2 w}{\partial x^2} + D_{22} \frac{\partial^2 w}{\partial y^2}) \right. \\ & \left. + 4D_{66} \frac{\partial^2 v}{\partial x \partial y} \frac{\partial^2 w}{\partial x \partial y} - v f \right\} d\Omega \\ & + \int_{\Omega_s} \left\{ I_0 v \frac{\partial^2 w}{\partial t^2} + I_2 \frac{\partial^2}{\partial t^2} \left(\frac{\partial v}{\partial x} \frac{\partial w}{\partial x} + \frac{\partial v}{\partial y} \frac{\partial w}{\partial y} \right) \right\} d\Omega \\ & + \int_{\Gamma_s} A d\Gamma - \int_{\Gamma_{sw}} \alpha v (w - \bar{w}) d\Gamma - \int_{\Gamma_{s\theta}} \beta \frac{\partial v}{\partial n} (\theta_n - \bar{\theta}) d\Gamma = 0 \end{aligned} \quad (18a)$$

and

$$\begin{aligned} A = & -v \left[\left(\frac{\partial M_x}{\partial x} + \frac{\partial M_{xy}}{\partial y} \right) n_x + \left(\frac{\partial M_{xy}}{\partial x} + \frac{\partial M_y}{\partial x^2} \right) n_y \right. \\ & \left. + I_2 \frac{\partial^2}{\partial t^2} \left(\frac{\partial v}{\partial x} n_x + \frac{\partial v}{\partial y} n_y \right) \right] + \frac{\partial v}{\partial x} (M_x n_x + M_{xy} n_y) \\ & + \frac{\partial v}{\partial y} (M_{xy} n_x + M_y n_y) \end{aligned} \quad (18b)$$

where M_x , M_y and M_{xy} are bending moments. (n_x, n_y) is the unit outward normal to domain Ω_s . M_x , M_y and M_{xy} can be expressed by the deflect, w , as

$$\begin{aligned} M_x = & -(D_{11} \frac{\partial^2 w}{\partial x^2} + D_{12} \frac{\partial^2 w}{\partial y^2}), \quad M_y = -(D_{12} \frac{\partial^2 w}{\partial x^2} + D_{22} \frac{\partial^2 w}{\partial y^2}), \\ M_{xy} = & -2D_{66} \frac{\partial^2 w}{\partial x \partial y} \end{aligned} \quad (19)$$

As shown in Fig. 2, the support sub-domain Ω_s of a node \mathbf{x}_i is a domain in which $v(\mathbf{x}) \neq 0$. An arbitrary shape support domain can be used, such as, a rectangular and circle support domains for thin plate problems. It can be found that the boundary Γ_s for the support domain Ω_s is usually composed by five parts: the internal boundary Γ_{si} , the boundaries Γ_{sw} , $\Gamma_{s\theta}$, Γ_{sM} , Γ_{sV} over which the essential boundary conditions w , θ and natural boundary conditions M , V are specified. The boundaries Γ_{sw} with Γ_{sV} and $\Gamma_{s\theta}$ with Γ_{sM} are mutually disjoint. Because the boundary conditions are often given on the local, normal and tangential, coordinates (n,s) , the derivatives in the integrations on the Γ_{sM} , and Γ_{sV} are converted to the coordinates (n,s) from the global coordinates (x,y) [Reddy

(1993)]. Imposing the natural boundary condition given in equation (4), we obtain:

$$\begin{aligned} & \int_{\Omega_s} \left\{ \frac{\partial^2 v}{\partial x^2} (D_{11} \frac{\partial^2 w}{\partial x^2} + D_{12} \frac{\partial^2 w}{\partial y^2}) + \frac{\partial^2 v}{\partial y^2} (D_{12} \frac{\partial^2 w}{\partial x^2} + D_{22} \frac{\partial^2 w}{\partial y^2}) \right. \\ & \left. + 4D_{66} \frac{\partial^2 v}{\partial x \partial y} \frac{\partial^2 w}{\partial x \partial y} - v f \right\} d\Omega \\ & + \int_{\Omega_s} \left\{ I_0 v \frac{\partial^2 w}{\partial t^2} + I_2 \frac{\partial^2}{\partial t^2} \left(\frac{\partial v}{\partial x} \frac{\partial w}{\partial x} + \frac{\partial v}{\partial y} \frac{\partial w}{\partial y} \right) \right\} d\Omega \\ & + \int_{\Gamma_{si}} A d\Gamma + \int_{\Gamma_{sw}} [A - \alpha v (w - \bar{w})] d\Gamma + \int_{\Gamma_{s\theta}} [A - \beta \frac{\partial v}{\partial n} (\theta_n - \bar{\theta}_n)] d\Gamma \\ & - \int_{\Gamma_{sM}} [v (\hat{Q}_n + \frac{\partial M_{ns}}{\partial s}) - \frac{\partial v}{\partial n} \bar{M}_n] d\Gamma - \int_{\Gamma_{sV}} [v \bar{V}_n - \frac{\partial v}{\partial n} M_n] d\Gamma = 0 \end{aligned} \quad (20)$$

where

$$\begin{aligned} M_n = & M_x n_x^2 + M_y n_y^2 + M_{xy} n_x n_y, \\ M_{ns} = & (M_y - M_x) n_x n_y + M_{xy} (n_x^2 - n_y^2), \\ \hat{Q}_n = & \left(\frac{\partial M_x}{\partial x} + \frac{\partial M_{xy}}{\partial y} \right) n_x \\ & + \left(\frac{\partial M_{xy}}{\partial x} + \frac{\partial M_y}{\partial y} \right) n_y + I_2 \frac{\partial^2}{\partial t^2} \left(\frac{\partial w}{\partial x} n_x + \frac{\partial w}{\partial y} n_y \right), \\ V_n = & \hat{Q}_n + \frac{\partial M_{ns}}{\partial s} \\ \frac{\partial}{\partial n} = & n_x \frac{\partial}{\partial x} + n_y \frac{\partial}{\partial y}, \quad \frac{\partial}{\partial s} = n_x \frac{\partial}{\partial y} - n_y \frac{\partial}{\partial x} \end{aligned} \quad (21)$$

For a support domain located entirely within the global domain, there is no intersection between Γ_s and the global boundary Γ . $\Gamma_{si} = \Gamma_s$, and the integrals over Γ_{sw} , $\Gamma_{s\theta}$, Γ_{sM} and Γ_{sV} vanish.

With equation (20) for every node \mathbf{x}_i , instead of dealing with a global problem equation (2), the problem becomes to deal with a localized problem over a local support domain.

5 Discretization and numerical implementation for the MLPG

5.1 Discrete equations of MLPG

The problem domain Ω is represented by properly scattered nodes. The Moving Least Squares approximation (9) is used to approximate the value of a point x_Q . Substituting equation (9) into the local weak form (20) for all

nodes leads to the following discrete system of equations:

$$\mathbf{M}\dot{\mathbf{w}}_e + \mathbf{K}\mathbf{w}_e = \mathbf{f} \quad (22)$$

where the “mass” matrix \mathbf{M} , the “stiffness” matrix \mathbf{K} and nodal “load” vector \mathbf{f} are defined by

$$\begin{aligned} m_{ij} &= \int_{\Omega_s} [I_0 v_i \phi_j + I_2 (v_{i,x} \phi_{j,x} + v_{i,y} \phi_{j,y})] d\Omega \\ &\quad - \int_{\Gamma_s - \Gamma_{sv}} I_2 v_i (\phi_{j,x} n_x + \phi_{j,y} n_y) d\Gamma \\ k_{ij}^{\Omega} &= k_{ij}^{\Omega} + k_{ij}^{\Gamma_{si}} + k_{ij}^{\Gamma_{sw}} + k_{ij}^{\Gamma_{s\theta}} + k_{ij}^{\Gamma_{sM}} + k_{ij}^{\Gamma_{sv}} \\ k_{ij}^{\Omega} &= \int_{\Omega_s} \{ v_{i,xx} (D_{11} \phi_{j,xx} + D_{12} \phi_{j,yy}) + v_{i,yy} (D_{12} \phi_{j,xx} + D_{22} \phi_{j,yy}) \\ &\quad + 4D_{66} v_{i,xy} \phi_{j,xy} \} d\Omega \\ k_{ij}^{\Gamma_{si}} &= \int_{\Gamma_{si}} B_{ij} d\Gamma, \\ k_{ij}^{\Gamma_{sw}} &= \int_{\Gamma_{sw}} (B_{ij} - \alpha v_i \phi_j) d\Gamma, \\ k_{ij}^{\Gamma_{s\theta}} &= \int_{\Gamma_{s\theta}} [B_{ij} - \beta v_{i,n} (\phi_{j,x} n_x + \phi_{j,y} n_y)] d\Gamma, \\ k_{ij}^{\Gamma_{sM}} &= \int_{\Gamma_{sM}} C_{ij} d\Gamma \\ k_{ij}^{\Gamma_{sv}} &= - \int_{\Gamma_{sv}} [v_{i,n} ((D_{11} \phi_{j,xx} + D_{12} \phi_{j,yy}) n_x^2 \\ &\quad + (D_{12} \phi_{j,xx} + D_{22} \phi_{j,yy}) n_y^2 + 4D_{66} \phi_{j,xy} n_x n_y)] d\Gamma \\ f_i &= \int_{\Omega_s} v_i f d\Omega - \int_{\Gamma_{sw}} \alpha v_i \bar{w}_n d\Gamma - \int_{\Gamma_{s\theta}} \beta v_{i,n} \bar{\theta}_n d\Gamma \\ &\quad - \int_{\Gamma_{sM}} v_{i,n} \bar{M}_n d\Gamma + \int_{\Gamma_{sv}} v_i \bar{V}_n d\Gamma \end{aligned} \quad (23a)$$

and

$$\begin{aligned} B_{ij} &= v_i [(D_{11} \phi_{j,xxx} + (D_{12} + 2D_{66}) \phi_{j,xyy}) n_x \\ &\quad + (D_{22} \phi_{j,yyy} + (D_{12} + 2D_{66}) \phi_{j,xyy}) n_y] \\ &\quad - v_{i,x} [(D_{11} \phi_{j,xx} + D_{12} \phi_{j,yy}) n_x + 2D_{66} \phi_{j,xy} n_y] \\ &\quad - v_{i,y} [2D_{66} \phi_{j,xy} n_x + (D_{12} \phi_{j,xx} + D_{22} \phi_{j,yy}) n_y] \\ C_{ij} &= v_i \{ [(D_{11} \phi_{j,xxx} + (D_{12} + 2D_{66}) \phi_{j,xyy}) n_x \\ &\quad + (D_{22} \phi_{j,yyy} + (D_{12} + 2D_{66}) \phi_{j,xyy}) n_y] \\ &\quad + n_x [(D_{12} \phi_{j,xyy} + D_{22} \phi_{j,yyy} - D_{11} \phi_{j,xyy} - D_{12} \phi_{j,yyy}) n_x n_y \\ &\quad + 2D_{66} \phi_{j,xyy} (n_x^2 - n_y^2)] + n_y [(D_{12} \phi_{j,xxx} + D_{22} \phi_{j,xyy} \\ &\quad - D_{11} \phi_{j,xxx} - D_{12} \phi_{j,xyy}) n_x n_y + 2D_{66} \phi_{j,xyy} \\ &\quad (n_x^2 - n_y^2)] \} \\ v_{i,n} &= v_{i,x} n_x + v_{i,y} n_y \\ w_e &= \{w_1, w_2, w_3, \dots, w_n\}^T \end{aligned} \quad (23b)$$

It can be easily seen that the system stiffness matrix \mathbf{K} in the present method is banded but asymmetric. For static analysis, the first term of equation (22) related time variable, t , vanishes. For free vibration, the loading, \mathbf{f} , vanishes and a linear eigenvalue equation needs be solved.

5.2 Weight function

As the MLPG is regarded as a weighted residual method, the weight function plays an important role in the performance of the method. In the integration on the boundaries of equation (18), 3r-order partial derivatives are used. There is not any problem if a weight function, v , with high continuity is used, such as equation (16). Theoretically, as long as the condition of continuity is satisfied, any weight function is acceptable. However, the local weak form is based on a local sub-domain of a node with the node at the center. It can be shown that weight functions which decrease in magnitude with increasing distance from the point x_Q to the node x_i yields better results. Therefore, weight functions which only depend on the distance between the two points are considered here. The 4th-order spline weight functions, equation (16), is used.

5.3 Numerical integration

A numerical integration is needed to evaluate the integration in equation (23). The Gauss quadrature is used in present work. For a node \mathbf{x}_i , a local integration cell is needed to employ Gauss quadrature. For each Gauss quadrature point \mathbf{x}_Q , the point interpolation is performed to obtain the integrand. Therefore, as shown in Fig. 2, for a node \mathbf{x}_i , there exist three local domains: local integration domain Ω_Q (size r_q), weight function domain Ω_v (same as Ω_s) for $v_i \neq 0$ (size r_v), and interpolation domain Ω_i for x_Q (size r_i). These three local domains are independent as long as the condition $r_q \leq r_v$ is satisfied. It should be noted that when the weight function equation (16) is used, the weight function v will be zero along the boundary of integration domain if the integration domain and weight domain are same ($r_q = r_v$). Equation (17) can be simplified because the integration along the internal boundary Γ_i vanishes. Hence, for simplification, we take $r_q = r_v$ in this paper. Because the problem domains in following examples are rectangle domains, rectangle sub-domains are used for establishing weight function. The size of the sub-domain (r_v) for node i and the size of the interpolation domain (r_i) are defined

$$r_v = \alpha_0 d_i \quad (24a)$$

$$r_i = \beta_0 d_i \quad (24b)$$

where, α_0 and β_0 are coefficients chosen. The d_i is the shortest distance between the node i and neighbor nodes. The effects of α_0 and β_0 will be investigated in following numerical examples.

There exist difficulties to obtain the exact numerical integration in meshless methods. It has been discussed in detail for 2-D solids by Atluri et al.(1999b). The numerical integration errors are results from the complexities of the integrand. Because the integrand of the plate analysis is more complex than 2-D plane problem, additional attentions should be paid for the numerical integration. In order to guarantee the accuracy of the numerical integration, the Ω_Q should be divided into some regular small sub-partitions. In each sub-partition, more Gauss quadrature points should be used.

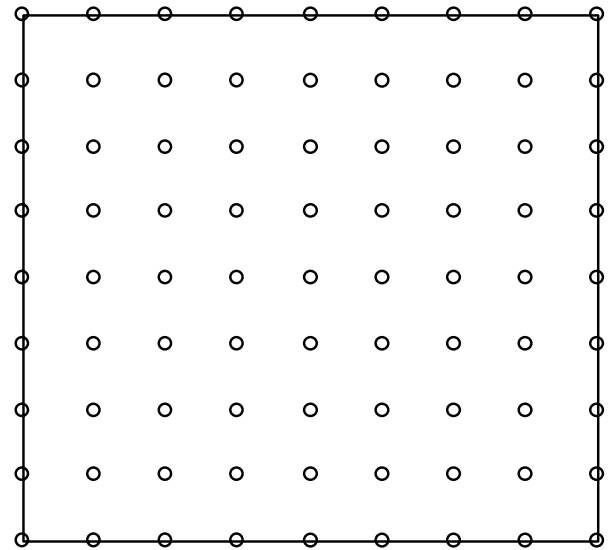
6 Numerical results

6.1 Static analysis of thin plates

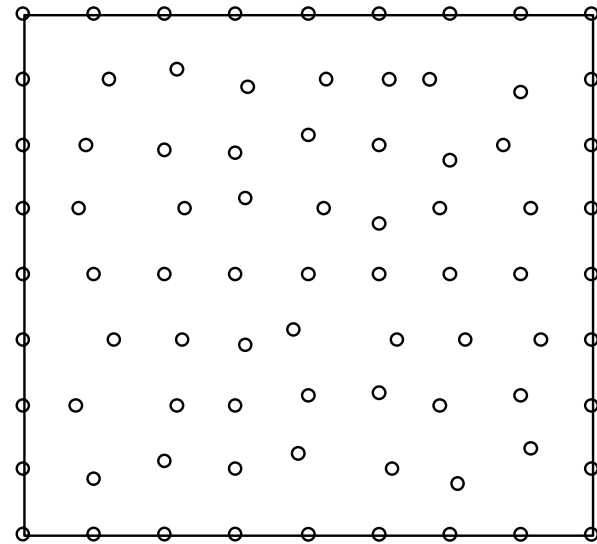
The MLPG method is used for static bending analysis of thin plates. Except special mentioned, in following examples for static analyses, the units are taken as standard international (SI) units, and the parameters are taken as thickness $t=1.0 \times 10^{-2}$, Young's modulus $E=2.1 \times 10^9$, Poisson ratio, $\nu = 0.3$. For the boundary conditions in the rectangular plates, 'S-S-S-S' denotes fully simple supported; 'C-C-C-C' denotes fully clamped; 'S-C-S-C' denotes two opposite edges simple supported and the other edges ($y=0, b$) clamped

6.1.1 Effects of parameters

Parameters on the performance of the present method are investigated first. The square plate under various loads is well-known benchmark with a large number of numerical and analytical solutions to compare with. The analytical results given by Timoshenko and Woinowsky-Krieger(1995) are used to compare with the present results. In following parameter investigations, the fully simply supported and clamped square plates are used. As shown in Fig.1, a square plate with $a=b=4$ is considered. Figure 3 shows two kinds of nodal arrangements with regular distributed 81 nodes and irregular distributed 81 nodes, respectively. Regular distributed 81 and 289 nodes are utilized in the following parameter investigations. The plate subject to a uniformly distributed load of $q=100$. The analytical solution is available and can be found in a textbook by Timoshenko and Woinowsky-Krieger(1995). The maximum deflection,



(a)



(b)

Figure 3 : Nodal arrangement for a square thin plate (a) regular distribution (b) irregular distribution

w_{max} , is located at the center of the plate:

$$w_{max} = C_0 \frac{a^4 q}{D_{11}} \tag{25}$$

The analytical results of C_0 for this case are 0.004062 for fully simply supported plates and 0.00126 for fully clamped plates.

a) Effects of local support domain

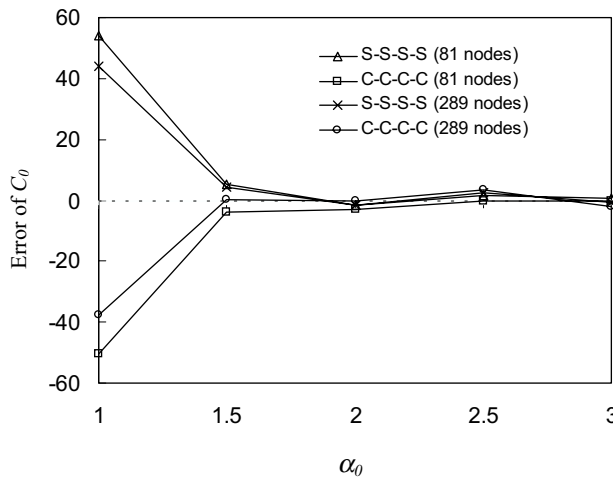


Figure 4 : Influence of parameter α_0 of the support domain

As the MLPG is a local meshless method, the size of the local support domain used will affect the accuracy of the solution. Several support domains with different sizes (r_v), which are determined by the parameter α_0 in equation (24a), are therefore investigated. The errors of the deflections (C_0) for two nodal arrangements are plotted in Fig. 4. From this figure, it can be found that the accuracy for deflections increases with the increase of the support domain size.

When the support domain is too small ($\alpha_0 = 1.0$), the results will become unacceptable. This is because a local residual formulation with very small support domain for the weight function behaves more like a strong form formulation. Strong form formulation is usually less accurate than a weak integral form formulation [Lu et al. (1994)], which integration smears the error over the integral domain.

When the support domain is big enough ($\alpha_0 \geq .5$), results obtained are very good. However, there exist difficulties to get accurate numerical integrations for a big

sub-support domain. When the support size becomes too large ($\alpha_0 \geq 0.3$), it can be found that the errors will increase a little due to increase of integration errors. For a big sub-support domain, more regular small partitions and Gauss quadrature points are needed to obtain accurate integrations. The numerical integration will become computationally expensive and not really necessary. Hence, $\alpha_0=2.0$ is an economic choice.

It may also be mentioned here that too large local support domain does not necessarily give a significant improvement on accuracy. This fact is clearly evidenced in Fig. 4. This fact implies that as long as the integral domain is large enough to “smear” the error, the size of integral domain does not play an important role.

b) Effects of interpolation domain

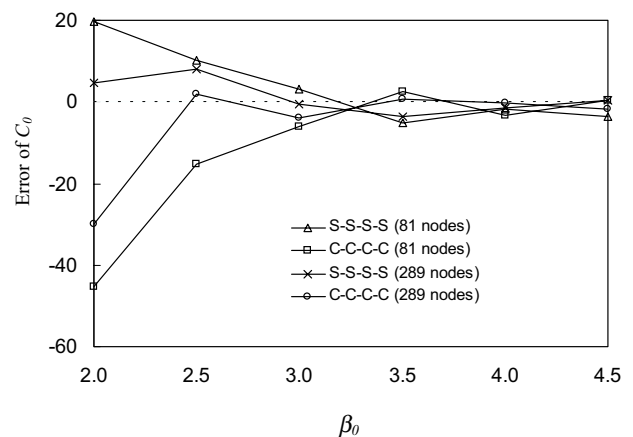


Figure 5 : Influence of parameter β_0 of the interpolation domain

The size of influence domain of a quadrature point is determined by the parameter β_0 in equation (24b). Because the problem domain is rectangular, rectangular influence domains are used. The errors of the deflections (C_0) of $\beta_0=2.0\sim 4.5$ are obtained and plotted in Fig. 5. It can be found that the accuracy for deflections increases with the increase of the influence domain size. Results of $\beta_0=3.0\sim 4.5$ (about 40~70 nodes used in a influence domain) are very good. A too small influence domain ($\beta_0 \leq 2.5$) leads large errors. The bad accuracy of a too small influence domain is because that there are not enough nodes (about less than 16 nodes) to perform interpolation for the field variable.

Using a too big influence domain will increase the computational cost in interpolation. Therefore, $\beta_0=3.0\sim 4.5$

can obtain an acceptable result. For convenience and consistency, $\beta_0=4.0$ will be used in the following studies.

c) Convergence study

The convergence of MLPG method is also investigated using regular distributed nodes. The following norm using C_0 is defined as an error indicator

$$e_C = |C_0 - \bar{C}_0| / \bar{C}_0 \quad (26)$$

where C_0 is the dimensionless deflection coefficient obtained by numerical method, and \bar{C}_0 is the analytical result.

The e_C with mesh refinement is shown in Fig. 6. Here, h is equivalent to the maximum element size in the FEM analysis. From Fig. 6, it can be observed that the convergence of MLPG method is very good.

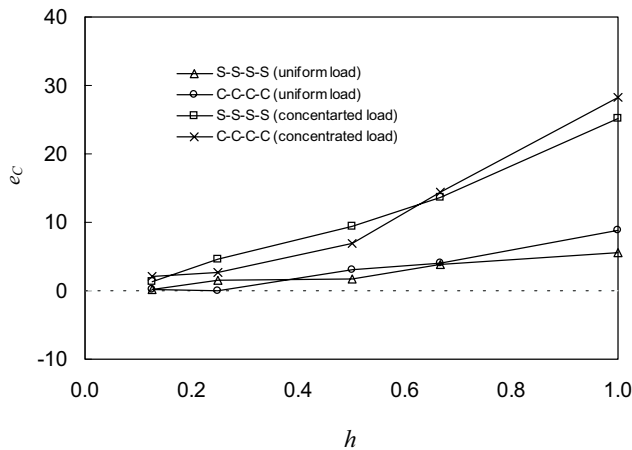


Figure 6 : Convergence in e_C norm of error

6.1.2 Comparison with other methods

Some researchers [Krysl and Belytschko (1995); Liu and Chen (2001)] have investigated the use of EFG method in analyses of thin plate problems. For comparison, a square thin plate subjected to concentrated force at the center is used. The dimensionless deflection coefficients C_0 are obtained using MLPG method and listed in table 1. EFG results [Liu and Chen (2001)] and FEM results are also listed in the same table. The regular nodal arrangement (169 nodes) is used in the MLPG and EFG analyses. A FEM software, ABAQUS, and 144 thin shell elements are used in the FEM analysis.

From this table, we can find that all these three methods can obtain very good results for this benchmark problem. The accuracy of MLPG is nearly same as EFG, and slightly lower than that of FEM. The reason seems because the effect of integration error. Although the accuracy of interpolation in MLPG and EFG is higher than that in FEM, bigger integration errors in MLPG and EFG will make a negatively influence of the results. However, FEM is more sensitive for the mesh distribution. For an irregular mesh, FEM tends to perform much worse, even fail. MLPG and EFG show much less pronounced loss of accuracy. Krysl and Belytschko (1995) and Liu and Chen (2001) obtained same conclusions in their papers. The robustness for an irregular nodal arrangement is a very important advantage of meshless methods.

The performance of MLPG method is also compared with EFG method and FEM. To solve a thin plate problem, the computational efficiency of MLPG is slightly lower than that of EFG. It is because an asymmetric system matrix has to be used in MLPG to solve the global system equation. FEM needs much shorter computational time than that of MLPG and EFG method. However, the computational time of FEM does not include the time for meshing. The meshing in FEM is usually very time-consuming and expensive. In the meantime, the requirement of background integration mesh in EFG method is also expensive and inconvenient. Therefore, as a truly meshless method, no mesh is needed in the present MLPG. It makes MLPG method is very efficient, especially for complicated application problems.

6.1.3 Square plate under different load with different support

Using above-mentioned parameters, deflections of a S-S-S-S square thin plate using regular nodal arrangement (81 nodes) obtained by MLPG is plotted in Fig. 7. The result obtained by analytical is also plotted in the Fig. 7(b). From this figure, one can observe that the result by the present MLPG method is in very good agreement with those obtained using the analytical method.

The irregular distribution nodal arrangement, shown in Fig 3(b), is also used for the static analysis. Deflection results are plotted in Fig. 7(b). From Fig. 7(b), one can observe that very good results are obtained using the irregular distribution nodal arrangement. The computational stability and high accuracy for a non-structured nodal distribution are very significant advantages of MLPG. These properties are very beneficial for practical appli-

Table 1 : Dimensionless deflection C_0 of a square plate using MLPG, EFG and FEM

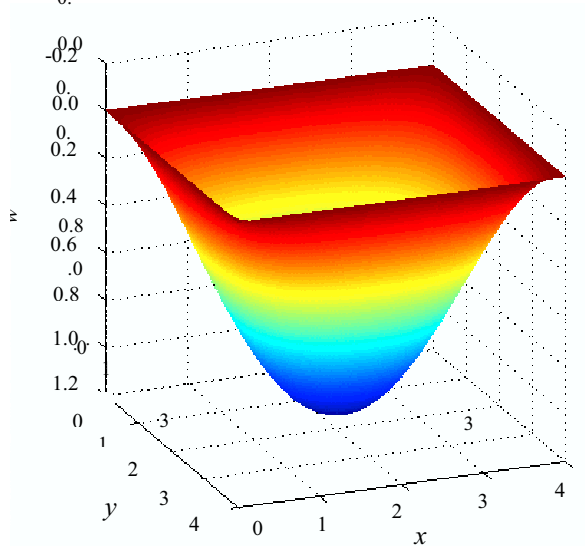
	MLPG	EFG (Liu and Chen, 2001)	FEM (ABAQUS)	Analytical
S-S-S-S	0.01107	0.01145	0.01151	0.01160
C-C-C-C	0.00584	0.00546	0.00552	0.00560

$$C_0 = w_{max}D/Pa^2$$

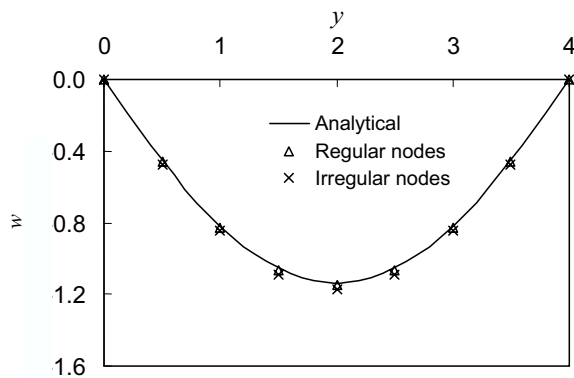
Table 2 : Dimensionless deflection C_0 of a square plate

	Uniform load*			Concentrated load**		
	S-S-S-S	CCCC	S-C-S-C	S-S-S-S	C-C-C-C	S-C-S-C
121 nodes	0.00399	0.00122	0.00188	0.01091	0.00598	0.00737
289 node	0.00400	0.00126	0.00196	0.01214	0.00575	0.00717
Analytical	0.00406	0.00126	0.00192	0.01160	0.00560	0.00704

* $C_0 = w_{max}D/qa^4$ for uniform load, * $C_0 = w_{max}D/Pa^2$ for concentrated load



(a)



(b)

Figure 7 : Deflection of the square plate (a) deflection field (b) deflection at the middle line ($x=2$)

cations.

Thin square plates under different distributed loads with different boundary conditions are also analyzed. Two loading cases (uniform load and a concentrated load on the plate center with $P=100$) and three support cases, S-S-S-S, C-C-C-C and S-C-S-C, are considered. The comparisons between the deflection results calculated analytically and using the MLPG are listed in table 2. Excellent agreements results between the analytical and numerical results are obtained.

6.1.4 Rectangular plate

The MLPG method is used to analyze thin plates of different ratios of length, a , and width, b . As shown in Fig. 1, a keeps unchanged ($a=4$). b is changed accordingly. The same nodal density is used for different ratios. Hence, h , equivalent to the maximum element size, keeps unchanged and number of nodes changed accordingly. Two nodal densities are used with $h=0.4$ and 0.25 , respectively. Dimensionless deflection coefficients of rectangular plates under different distributed loads with different boundary conditions are listed in table 3. For comparison, analytical results are also listed in the same table. From this table, one can observe that very good results can be obtained using MLPG for rectangular plates.

6.1.5 Circular plate

MLPG is also used to analyze a fully simply supported and clamped thin circular plate (Fig. 8) subjected to uniform transverse pressure q . The deflection along the radial section is given for the thin circle plate:

$$w = \frac{q(a^2-r^2)}{64D_{11}} \left(\frac{5+\nu}{1+\nu} a^2 - r^2 \right) \quad \text{with simply supported edges}$$

Table 3 : Dimensionless deflection coefficients of a rectangular plate

Uniform load*									
b/a	S-S-S-S			C-C-C-C			S-C-S-C		
	h=0.4	h=0.25	Analytical	h=0.4	h=0.25	Analytical	h=0.4	h=0.25	Analytical
1.0	0.00399	0.00400	0.00406	0.00122	0.00126	0.00126	0.00188	0.00196	0.00192
1.2	0.00577	0.00558	0.00564	0.00170	0.00172	0.00172	0.00315	0.00317	0.00319
1.4	0.00701	0.00701	0.00705	0.00203	0.00206	0.00207	0.00458	0.00458	0.00460
1.6	0.00825	0.00823	0.00830	0.00226	0.00229	0.00230	0.00598	0.00599	0.00603
1.8	0.00925	0.00928	0.00931	0.00240	0.00243	0.00245	0.00729	0.00728	0.00732
2.0	0.01008	0.01013	0.01013	0.00248	0.00252	0.0254	0.00845	0.00841	0.00840

Concentrated load**									
b/a	S-S-S-S			C-C-C-C			S-C-S-C		
	h=0.4	h=0.25	Analytical	h=0.4	h=0.25	Analytical	h=0.4	h=0.25	Analytical
1.0	0.01091	0.01214	0.01160	0.00598	0.00575	0.00560	0.00737	0.00717	0.00704
1.2	0.01405	0.01410	0.01353	0.00664	0.00649	0.00647	0.00986	0.00979	0.00945
1.4	0.01571	0.01536	0.01484	0.00711	0.00694	0.00681	0.01207	0.01203	0.01157
1.6	0.01659	0.01637	0.01570	0.00730	0.00712	0.00712	0.01401	0.01379	0.01326
1.8	0.01710	0.01687	0.01620	0.00721	0.00739	0.00720	0.01518	0.01502	0.01450
2.0	0.01721	0.01701	0.01651	0.00723	0.00742	0.00722	0.01616	0.01580	0.01537

* $C_0 = w_{max}D/qa^4$ for uniform load ** $C_0 = w_{max}D/Pa^2$ for concentrated load

Table 4 : Dimensionless deflection coefficients C_0 of a circular plate

	Simply supported	Clamped
18 nodes	0.06712	0.01478
193 nodes	0.06513	0.01527
321 nodes	0.06391	0.01556
Analytical	0.06370	0.01562

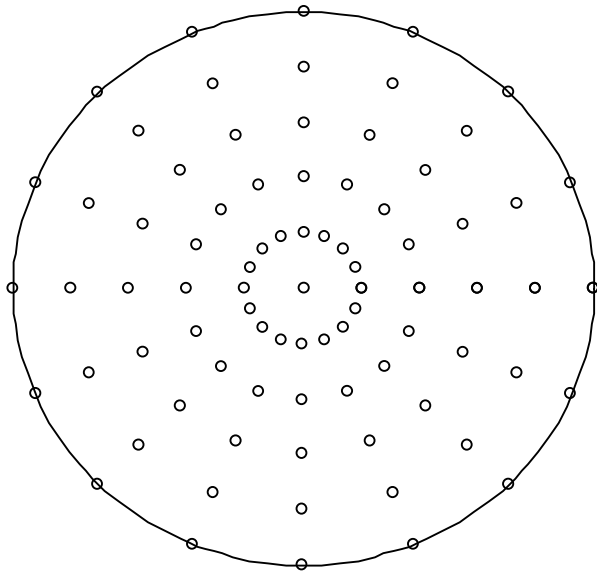


Figure 8 : Nodal arrangement for a circular plate

$$w = \frac{q}{64D_{11}}(a^2 - r^2)^2 \quad \text{with clamped edges,} \quad (27)$$

where a is the radius of the plate. The maximum deflection, w_{max} , located at the center of the plate is $w_{max} = C_0qa^4/D$. For $\nu=0.3$, the analytical results of C_0 are 0.06370 and 0.01562 for simply supported and clamped circle plates, respectively. The data used for the present analysis is: $a=2.0$, $q=100$. The comparisons between the deflection results calculated analytically and using the MLPG are listed in table 4. It can be found that a good result can be obtained by MLPG method for circular thin plates.

6.2 Free vibration analysis of thin plates

Consider now a square plate with following parameters: $a=b=10m$, $h=0.05m$, $E=2 \times 10^{11}N/m^2$, $\nu=0.3$ and $\rho 8000$

Table 5 : Natural frequencies (Hz) of lateral free vibration of a free square plate

Mode	Analytical solutions*	MLPG			FEM*	
		81 node	289 nodes	441 nodes	HOE**	LOE***
4	1.622	1.6552	1.6313	1.6234	1.532	1.632
5	2.360	2.4669	2.3396	2.3507	2.356	2.402
6	2.922	3.0399	2.9603	2.9444	2.861	3.006
7	4.233	4.3290	4.2813	4.2733	4.122	4.251
8	4.233	4.3290	4.2813	4.2733	4.122	4.251
9	7.416	7.8145	7.5917	7.4644	7.363	7.859
10	7.416	7.8145	7.5917	7.4644	7.363	7.859

*results from Abbassian et al. (1987)

**HOE: eight-node semi-loof thin sheel element (4 x 4 mesh)

***LOE: four-node iso-parametric shell element (8 x 8 mesh)

Table 6 : Natural frequencies (Hz) of lateral free vibration of S-S-S-S and C-C-C-C square plates

Mode	Analytical solutions	MLPG (regular nodes)			MLPG (irregular nodes)
		81 nodes	289 nodes	441 nodes	81 nodes
S-S-S-S plate*					
1	2.377	2.3938	2.3886	2.3815	2.3645
2	5.942	6.2042	5.9851	5.9629	6.1336
3	5.942	6.2042	5.9851	5.9629	6.4473
4	9.507	9.7235	9.5884	9.5564	10.0679
5	11.884	12.7908	12.1218	12.0049	12.5034
6	11.884	12.8753	12.1240	12.0064	12.8266
7	15.449	15.8641	15.6733	15.5824	15.6306
8	15.449	15.8641	15.6733	15.5824	16.1682
9		19.2520	20.8034	20.5548	19.5129
10		19.2510	20.8034	20.5548	19.9391
CCCC plate**					
1	4.333	4.4235	4.3455	4.3426	4.3797
2	8.839	8.7535	8.8843	8.8669	8.4847
3	8.839	8.7535	8.8843	8.8669	8.8120
4	13.040	13.0986	13.0940	13.0668	12.9692
5	15.845	15.1527	15.8834	15.9034	14.6923
6	15.918	15.1883	15.9585	15.9789	15.3032
7		19.9624	19.9344	19.9285	19.7194
8		19.9624	19.9344	19.9285	20.0986
9		24.7665	25.2571	25.3951	24.3576
10		24.7665	25.2571	25.3951	24.3576

* the analytical results from Abbassian et al. (1987)

** the analytical results from Robert (1979)

Kg/m³.

A fully free square plate is analyzed first. Three regular nodal arrangements are used. Frequencies obtained by MLPG method are listed in table 5. The analytical results and FEM results are also listed in the same table. The first three frequencies corresponding to the rigid movement are zero. From the table, one can observe that the present results show good agreements with analytical results and FEM results. The convergence is also demonstrated in this table. As the number of nodes increases, the result obtained approaches the analytical solution.

Natural frequencies of fully simply supported and fully clamped plates are obtained and listed in table 6. Three regular distributed arrangements and one irregular distributed nodal arrangement are used. It can be found that a good result can be obtained by MLPG method for free vibration analyses of these square plates. One can also observe that very good results are also obtained by MLPG method using the irregular distribution nodal arrangement.

7 Discussion and conclusions

The MLPG formulation for static and free vibration analyses of thin plates is presented in this paper. Local weak forms are developed from the 4th-order partial differential equation of Kirchhoff plates. The MLS approximation is used to obtain the shape functions. The satisfaction of the high continuity requirements is easily met by MLS interpolant.

Some important parameters on the performance of the present method are investigated in great detail. From the studies in this paper, the following conclusion can be drawn. When the local support domain is big enough ($\alpha_0 \geq 1.5$), results obtained are very good. $\alpha_0 = 2.0$ is recommended. The size of influence domain of $\beta_0 = 3.0 \sim 4.5$ should be used for most problems studied. The present method is compared with EFG method and FEM. It is found that the present method is robust and efficient.

Numerical examples are presented to demonstrate the convergence, validity and efficiency of the present method. The results presented are indeed very encouraging. It is demonstrated that the MLPG is easy to implement, and very flexible for static and free vibration analyses of Kirchhoff plates.

Reference

- Abbassian F, Dawswell DJ, Knowles NC** (1987) *Free vibration benchmarks*. Glasgow: National Engineering Laboratory
- Atluri SN, Cho JY, Kim HG** (1999a) Analysis of thin beams, using the meshless local Petrov-Galerkin (MLPG) method, with generalized moving least squares interpolation. *Computational Mechanics* 24: 334-347
- Atluri SN, Kim HG, Cho JY** (1999b) A critical assessment of the truly meshless local Petrov-Galerkin (MLPG), and Local Boundary Integral Equation (LBIE) methods. *Computational Mechanics* 24:348-372
- Atluri SN, Zhu T** (1998) A new meshless local Petrov-Galerkin (MLPG) approach in computational mechanics. *Computational Mechanics* 22:117-127.
- Atluri SN, Zhu T** (2000a) New concepts in meshless methods. *Int. J. Numer. Methods Engrg.* 47 (2000) 537-556.
- Atluri SN, Zhu T** (2000b) The meshless local Petrov-Galerkin (MLPG) approach for solving problems in elsto-statics. *Computational Mechanics* 225:169-179
- Belytschko T, Lu YY, Gu L** (1994) Element-Free Galerkin methods. *Int. J. Numer. Methods Engrg.* 37:229-256
- Belytschko T, Organ D** (1995) Coupled finite element-free Galerkin method. *Computational Mechanics* 17:186-195
- Ching H. C., Batra R. C.** (2001) Determination of crack tip fields in linear elastostatics by meshless local Petrov-Galerkin (MLPG) method. *CMES: Computer Modeling in Engineering & Sciences*, Vol. 2., No. 2.
- Gu YT, Liu GR** (2001a) A coupled element free Galerkin/boundary element method for stress analysis of two-dimensional solids. *Comput. Methods Appl. Mech. Engrg.* 190, 4405-4419
- Gu YT, Liu GR** (2001b) A meshless local Petrov-Galerkin (MLPG) method for free and forced vibration analyses for solids. *Comp. Mech.* 27, 188-198
- Kim HG, Atluri SN** (2000) Arbitrary placement of secondary nodes and error control in the meshless local Galerkin (MLPG) method. *CMES: Computer Modeling in Engineering & Sciences*, Vol. 1., No. 3.: 11-32
- Krysl P, Belytschko T** (1995) Analysis of thin plates by the element-free Galerkin method, *Comp. Mech.* 17: 26-

35

- Lancaster P, Salkauskas K** (1981) Surfaces generated by moving least squares methods. *Math. Comput.* 37, 141-158.
- Lin H, Atluri S. N.** (2000) Meshless Local Petrov-Galerkin (MLPG) method for conection-difusion problems. *CMES: Computer Modeling in Engineering & Sciences*, Vol. 1., No. 2.: 45-60
- Lin H, Atluri S. N.** (2001) The Meshless Local Pektrov-Galerkin (MLPG) Method for solving Incompressible Navier-Stokes Equations. *CMES: Computer Modeling in Engineering & Sciences*, Vol. 2., No. 2.: 117-142
- Liu G. R.** (1999) A Point Assembly Method for Stress Analysis for Solid. In: *Shim VPW(ed) Impact Response of Materials & Structures*. Oxford, 475-480
- Liu G. R., Chen X. L.** (2001) A mesh-free Galerkin method for static and free vibration analyses of thin plates of complicated shape. *Journal of Sound and Vibration*. 241 (5), 839-855
- Liu GR, Gu YT** (2000a) Coupling Element Free Galerkin and Hybrid Boundary Element methods using modified variational formulation. *Computational Mechanics* 26 (2): 166-173
- Liu G. R., Gu Y. T.** (2000b) Meshless local Petrov-Galerkin (MLPG) method in combination with finite element and boundary element approaches, *Computational Mechanics* 26 (6): 536-546
- Liu G. R., Gu Y. T.**(2001a) A Point Interpolation Method for two-dimensional solid. *Int. Journal for Numerical Methods in Eng.* 50: 937-951
- Liu G. R., Gu Y. T.**(2001b) A Local Point Interpolation Method for stress analysis of two-dimensional solids. *Structural Engineering and Mechanics* 11 (2): 221-236
- Liu WK, Jun S, Zhang YF**(1995) Reproducing kernel particle methods. *Int. J. Numer. Methods Engrg.* 20: 1081-1106.
- Lu Y. Y., Belytschko T., Gu L.**(1994) A new implementation of the element free Galerkin method. *Comput. Methods Appl. Mech. Engrg.* 113, 397-411.
- Mukherjee YX, Mukherjee S** (1997) Boundary node method for potential problems. *Int. J. Num. Methods in Engrg.* 40: 797-815.
- Nayroles B, Touzot G, Villon P** (1992) Generalizing the finite element method: diffuse approximation and diffuse elements. *Comput. Mech.* 10: 307-318.
- Oñate, Idelsohn E. S., Zienkiewicz O. C., Tylor R. L.** (1996) A Finite Point method in computational mechanics. Applications to connective transport and fluid flow. *Int. J. Numer. Methods Engrg.* 39 (22), 3839-3867.
- Reddy JN** (1993) *An introduction to the Finite Element Method*. New York: McGraw Hill, 2nd edition
- Robert DB** (1979) *Formulas for natural frequency and mode shape*. New York: Van Nostrand Reinhold Company
- Timoshenko S, Woinowsky-krieger S** (1995) *Theory of plates and shells*. New York: McGraw Hill, 2nd edition
- Wordelman C. J., Aluru N. R., Ravaioli U.** (2000) A meshless method for the numerical solution of the 2 and 3-D semiconductor Poisson equation. *CMES: Computer Modeling in Engineering & Sciences*, Vol. 1., No. 1.: 121-126
- Zhu T, Zhang JD, Atluri SN** (1998) A local boundary integral equation (LBIE) method in computational mechanics, and a meshless discretization approach. *Computational Mechanics* 21:223-235